

Palladium Nanoparticles Loaded on Carbon Modified TiO₂ Nanobelts for Enhanced Methanol Electrooxidation

Robert Liang^{1,2}, Anming Hu^{1,*}, John Persic³, Y. Norman Zhou^{1,2}

(Received 18 July 2013; accepted 30 August 2013; published online 12 September 2013)

Abstract: Carbon modified TiO₂ nanobelts (TiO₂-C) were synthesized using a hydrothermal growth method, as a support material for palladium (Pd) nanoparticles (Pd/TiO₂-C) to improve the electrocatalytic performance for methanol electrooxidation by comparison to Pd nanoparticles on bare TiO₂ nanobelts (Pd/TiO₂) and activated carbon (Pd/AC). Cyclic voltammetry characterization was conducted with respect to saturated calomel electrode (SCE) in an alkaline methanol solution, and the results indicate that the specific activity of Pd/TiO₂-C is 2.2 times that of Pd/AC and 1.5 times that of Pd/TiO₂. Chronoamperometry results revealed that the TiO₂-C support was comparable in stability to activated carbon, but possesses an enhanced current density for methanol oxidation at a potential of -0.2 V vs. SCE. The current study demonstrates the potential of Pd nanoparticle loaded on hierarchical TiO₂-C nanobelts for electrocatalytic applications such as fuel cells and batteries.

Keywords: Titanium oxide nanobelts; Carbon-modification; Fuel cell; Methanol electrooxidation; Palladium nanoparticles; Electrocatalysts

Citation: Robert Liang, Anming Hu, John Persic and Y. Norman Zhou, "Palladium Nanoparticles Loaded on Carbon Modified TiO₂ Nanobelts for Enhanced Methanol Electrooxidation", *Nano-Micro Lett.* 5(3), 202-212 (2013). <http://dx.doi.org/10.5101/nml.v5i3.p202-212>

Introduction

Direct methanol fuel cells (DMFC) have garnered interest in the portable devices and transportation industries because of their relatively low cost, high storage capabilities, low temperature operation, low-carbon emission, and high energy density [1-3]. However, issues pertaining to sluggish catalytic kinetics and instability of methanol delivery systems due to poisoning, limit their potential practical applications [4-6]. Recently, substantial work has been devoted towards electrooxidation of alcohols using platinum (Pt)-based catalysts in alkaline medium [7-10]. However, the activity of alcohol electrooxidation on many Pt-based catalysts in

alkaline medium is hindered by two factors: i) the high cost of Pt because of low supply and high demand in industry and ii) the propensity of Pt catalysts to strongly absorb carbon monoxide (CO_{ads}) intermediates, while having difficulty in oxidizing adsorbed CO into CO₂. This inability to oxidize CO_{ads} hampers the catalytic activity [11,12].

As a substitute to Pt, palladium (Pd) has been demonstrated to be a suitable electrocatalyst for DMFC. At present, there are many efforts to enhance the electrocatalytic activity of Pd through the improvement of its geometrical and electronic properties. A common strategy is combining Pd with other metals forming alloys, such as PdSn, PdRu, and PdNi [13-15].

¹Centre for Advanced Materials Joining, Department of Mechanical and Mechatronics Engineering, University of Waterloo, 200 University Avenue West, Waterloo, ON, N2L 3G1, Canada

²Waterloo Institute for Nanotechnology, University of Waterloo, 200 University Avenue West, Waterloo, ON, N2L 3G1, Canada

³Microbonds Inc., 151 Amber St., Unit 12, Markham ON, L3R 3B3, Canada

*Corresponding author: E-mail: anming.hu@uwaterloo.ca

Alloy catalysts have a higher oxygen reduction activity than pure Pd [15], which help promote the oxidation of strongly adsorbed intermediates, such as the oxidation of CO_{ads} to CO_2 . Another effective strategy is to prepare composite catalysts by coupling with semiconducting oxides (TiO_2 , SnO_2 and RuO_2) as support materials, which have been demonstrated to improve the catalytic activity and stability of Pd catalyst for alcohol electrooxidation [6,16,17]. Among these metal oxides, TiO_2 is touted as an effective substrate because of its high catalytic activity, long-term stability, and non-toxicity [18,19]. However, there are significant drawbacks of using TiO_2 , which include poor electrical conductivity.

TiO_2 nanobelts, previously used for photocatalysis in water treatment [20-22], were adopted for the use in electrocatalyst supports for Pd nanoparticles (denoted as Pd/ TiO_2). In order to increase the conductivity of the electrocatalyst support, the surface was modified with a thin layer of carbon using glucose as a carbon precursor source. A similar study has been conducted on Pd loaded on carbonized TiO_2 nanotubes for alcohol electrooxidation [23]. Furthermore, there have been other studies that use TiO_2 on carbon fibers [24,25], nanotubes [26-28], and nanoparticles [29] for electrocatalysts. To the best of our knowledge, carbonized anatase TiO_2 nanobelts have not yet been researched as a support for Pd catalysts for electrooxidation.

In this paper, we have conducted preliminary work on improving the conductivity of TiO_2 nanobelt supports via carbonization and demonstrate higher peak density currents for methanol electrooxidation than the study conducted by F. Hu *et al.*, which used carbonized TiO_2 nanotubes [23]. The electrocatalytic activities of Pd/ TiO_2 -C toward methanol electrooxidation were conducted using an electrochemical cell with a three-electrode setup and compared to Pd nanoparticles loaded on bare TiO_2 nanobelts (Pd/ TiO_2) and on activated carbon (Pd/AC).

Experimental

Synthesis of TiO_2 nanobelts and carbon modified TiO_2 nanobelts

TiO_2 nanobelts were synthesized using a modified hydrothermal process reported in a previous work [20-22]. In a beaker, 2.0 g of TiO_2 nanoparticle precursor (P25 AeroxideTM, Evonik Industries, particle size: 21 nm, BET surface area: $50 \pm 15 \text{ m}^2/\text{g}$) was dispersed in 60 mL of 10 M NaOH. The solution was stirred in a beaker until well mixed and transferred to a 100 mL Teflon-lined autoclave and heated at 190°C for 72 hours. The product was filtered and washed in distilled water for several times, including an acid wash in 0.1 M HCl solution until $\text{pH} = 7$. $\text{H}_2\text{Ti}_3\text{O}_7$ nanobelts were subse-

quently obtained and dried at 70°C overnight. Bare TiO_2 nanobelts were obtained by calcining $\text{H}_2\text{Ti}_3\text{O}_7$ nanobelts at 450°C for 3 hours in air in a furnace. The powder was then ramped to 700°C at a rate of 10°C/min and held for an hour to form bare TiO_2 nanobelts.

TiO_2 -C nanobelts were obtained using a modified version of a method reported elsewhere [30]. In short, 0.75 g of as-prepared $\text{H}_2\text{Ti}_3\text{O}_7$ nanobelts was easily dispersed by ultrasonication in 60 mL aqueous solution with 1.44 g of glucose. The solution was then transferred to a 100 mL Teflon-lined autoclave and heated to 180°C and held for 4 hours. After cooling overnight, these suspensions were harvested by filtration and washed with deionized water and ethanol alternately at least five times. After drying at 70°C, the resulting brown products were carbonized at 450°C for 3 hours under nitrogen atmosphere in a tube furnace. The powder was then ramped to 700°C at a rate of 10°C/min and held for an hour to form TiO_2 -C nanobelts.

Synthesis of Pd/ TiO_2 -C nanobelt catalysts

Pd nanoparticles were loaded on as-prepared TiO_2 -C nanobelts, TiO_2 nanobelts, and activated carbon (AC) through a liquid phase reduction method [31]. In a typical procedure, 6.8 mL of 40 mM of Na_2PdCl_4 (99.995% trace metals basis, Sigma Aldrich) aqueous solution and 120 mg TiO_2 -C nanobelts were added to 50 mL water. The pH was adjusted to 9 using NaOH and the suspension was stirred for 2 hours. After 2 hours, 100 mL 0.05 M NaBH_4 reductant was added dropwise to the solution. The obtained suspension was magnetically stirred for an additional hour. Subsequently, the mixture was centrifuged at 3000 RPM, filtered in vacuum and rinsed using Millipore water. The resultant product was dried in a furnace at 70°C overnight. The same liquid phase reduction method was used to form Pd nanoparticles that were supported on bare TiO_2 nanobelts and activated carbon (Glassy spherical powder: 99.95% trace metals basis and $>100 \text{ m}^2/\text{g}$ specific surface area, Sigma Aldrich). The final amount of Pd loaded in each sample was determined by anodic stripping voltammetry (see Fig. S3) and the results are shown in Table 1.

Microstructure and chemical composition characterization

The carbon content of the TiO_2 -C composite was investigated using thermogravimetric analysis (TGA, TA Instruments Q500) from 50°C to 800°C at a rate of 10°C under air flow (60 mL/min). The phase and microstructure of as-synthesized TiO_2 nanobelts and TiO_2 -C nanobelts were investigated using Raman spectroscopy, X-ray diffraction (XRD), field emission scanning electron microscopy (FE-SEM), high resolution transmission electron microscopy (HRTEM) and X-

ray photoelectron spectroscopy (XPS). Raman spectroscopy was conducted using a Raman microscope (Renishaw in via microscope equipped with 488 nm Ar ion laser and a grating of 2400 L/mm) with a spectral resolution of $< 1 \text{ cm}^{-1}$. The morphology of the as-synthesized TiO_2 nanobelts was evaluated using a ZEISS LEO 1530 FE-SEM equipped with energy dispersive X-ray (EDX) instrument at an accelerating voltage of 10 kV. Powder XRD measurements were performed on a Rigaku SA-HF3 X-ray diffractometer using Cu-K radiation (1.54 \AA) X-ray source equipped with an 800 μm collimator, operating at a voltage of 50 kV. The obtained diffraction patterns were collected from 10° to 120° at a scanning rate of $1.5^\circ/\text{min}$. HRTEM observation was conducted using a JEOL 2010F at the Canadian Centre for Electron Microscopy (Hamilton, Ontario, Canada). TEM samples were prepared by suspending TiO_2 nanobelts in ethanol and drip casting the solution onto lacey carbon grids. X-ray photoelectron spectroscopy (XPS) measurements were used to verify TiO_2 , carbon, and Pd contents. The measurement was carried out in ultra-high vacuum (HV) equipped with VG Scientific ESCALab 250, using an aluminum $K\alpha$ X-ray radiation source ($h\nu = 1486.6 \text{ eV}$). High resolution spectra were collected with a dwell time of 0.1 s per point for all scans. Survey scans were collected at 50 eV pass energy, whereas individual scans were collected at 20 eV pass energy. C1s, Ti2p, O1s, C1s, and Pd3d regional spectra were obtained and their peaks deconvoluted.

Table 1 Pd (II) concentrations of Pd/ TiO_2 , Pd/ TiO_2 , and Pd/AC catalysts obtained from anodic stripping voltammetry.

| Sample | Sample Concentration (mg/mL) | Pd Concentration (mg/mL) | Std. Error | Pd in Sample (%) |
|-----------------------|------------------------------|--------------------------|------------|------------------|
| Pd- TiO_2 -C | 11.1 | 1.35 | 0.040 | 12.2 \pm 0.4 |
| Pd- TiO_2 | 12.4 | 2.09 | 0.062 | 16.9 \pm 0.5 |
| Pd-AC | 11.0 | 1.41 | 0.042 | 12.8 \pm 0.4 |

* Sample size ($n = 3$) and a dilution factor of 1000 was used when running anodic stripping voltammetry tests in order to interpolate Pd concentration from calibration curve

Conductivity measurements

A modified method by Y. L. Hsin *et al.* was used to determine conductivity of powdered catalysts [32]. The powder samples of TiO_2 -C, TiO_2 , and AC were packed into heat-shrink tubing (diameter: 3.18 mm, 18 mm length) with two #4 stainless steel screws (2.78 mm diameter). One end of the tubing was capped with a screw before packing the powder samples, and subsequently shrunk to tightly fit onto the screw end using a hot air blower. Powder samples were added into the open end of the tubing and compressed until densely

packed. Subsequently, the open end of the tubing was capped off with another screw and heat shrunk to fit the screw.

The DC electrical resistance of the pressed powder was determined by a two-probe method. A known current was applied to the sample in one direction, then in the opposite one via two #4 screw end terminals. The real voltage drop was calculated from the arithmetic mean of two voltage drop values, in order to correct for thermo-electric contributions. A Keithley 2400 Source-meter was used as a current supply and voltage measurement meter. In each experiment, several values of current were measured to ensure ohmic behavior of the sample. The resistances of the #4 stainless steel screws were much lower than that of the powder samples used in this study.

Electrochemical measurements

Electrochemical measurements were conducted using a three-electrode setup, consisting of the catalyst on a working electrode, Pt wire as the counter electrode, and a saturated calomel electrode (SCE, 0.242 V vs. normal hydrogen electrode) as the reference electrode. The catalyst ink for the working electrode was prepared by dispersing 5 mg of catalyst in 2 mL H_2O and sonicating for 10 min. A volume of 12 μL of prepared catalyst ink was dispersed onto a glassy carbon electrode (GC, 3 mm diameter, CH Instruments Inc.), which served as the working electrode. After drying the ink at room temperature, 2 μL of Nafion (5 wt% in lower aliphatic alcohols and water, Sigma-Aldrich) was applied on the GC electrode. This setup was used in measurements to determine Pd concentration of the catalysts and methanol electrooxidation performance.

The catalysts were digested using aqua regia and the Pd concentration of the catalysts were determined by anodic stripping voltammetry using a glassy carbon electrode modified with chitosan (see Experimental Details – Preparation of Chitosan Modified Electrode in the ESI) in 0.02 M KCl-HCl supporting electrolyte (pH 2.0). Pd (II) standard solutions were developed from PdCl_2 and a calibration curve was constructed to determine the Pd concentration of the catalysts (see Experimental Details – Pd (II) Concentration Characterization in the ESI). Anodic stripping voltammetry was conducted from a potential range from 0.0 V to 1.0 V at a scan rate of 100 mV/s. Additionally, the working electrode was conditioned at a potential at 0.0 V for 60 s before measurement and an accumulation time of 60 s was used. High-purity nitrogen was used to deaerate the solution for 15 min and the measurements were carried out under an atmosphere of nitrogen at room temperature.

Base cyclic voltammetry (CV) experiments were carried out in a 1 M KOH solution at a scan rate of 50

mV/s. Cyclic voltammetry was conducted in 1 M KOH and varying concentrations of methanol (0.1 M to 4.0 M) at a scan rate of 50 mV/s. Chronoamperometry was conducted at -0.2 V vs. SCE in 1 M KOH + 1.0 M methanol (MeOH). All the above electrochemical measurements were performed on the PSTAT500Gamry Instrument Potentiostat. Furthermore, all tests were purged under nitrogen for 10 min before starting any experiment and potentials were quoted with respect to SCE. All tests were reproduced five times and are within 5% error. In addition, current densities were normalized by the electrochemical active surface area (EASA), or specific activity. The EASA of the catalysts were determined by integrating the charge (Q) on the PdO reduction peak region and using the equation [33],

$$EASA = \frac{Q}{Sl} \quad (1)$$

where S is the proportionality constant used to relate charge with area and l is the Pd catalyst loading in mg. A charge value of $405 \mu\text{C}/\text{cm}$ for reduction of the PdO monolayer was used [34].

Results and discussion

Material characterization and analysis

Thermogravimetric analysis was used to analyze the

weight composition of carbon in $\text{TiO}_2\text{-C}$ from 50°C to 800°C . From the analysis, the $\text{TiO}_2\text{-C}$ nanobelts contained 12.8% carbon by weight (Fig. S1). TiO_2 remains stable beyond the maximum temperature of the experimental run so the mass loss can be attributed solely to the thermal oxidation of the carbon material. It is important to point out that the high retention of Pd particles (greater than 85%) after centrifugation at 3000 RPM and filtration suggests that the particles are properly impregnated on the supports rather than simply mixed.

The Raman spectra shown in Fig. S2 reveal the existence of 3 characteristic anatase bands of $392 \text{ cm}^{-1}(B_{1g})$, $512 \text{ cm}^{-1}(A_{1g})$, and $634 \text{ cm}^{-1}(E_g)$ [35]. The $\text{TiO}_2\text{-C}$ spectrum reveals the existence of two carbon bands, one at 1348 (D) cm^{-1} and the other at 1589 (G) cm^{-1} [36], corresponding to defect and graphitic bands of carbon, respectively; it also depicts the three characteristic anatase bands- $389 \text{ cm}^{-1}(B_{1g})$, $508 \text{ cm}^{-1}(A_{1g})$, and $630 \text{ cm}^{-1}(E_g)$ – that are similar to bare TiO_2 nanobelts, however they are red-shifted by $3\text{-}4 \text{ cm}^{-1}$ indicating that there is an interaction with the surface carbon due to Raman spectroscopy being sensitive to crystallinity and microstructure of a material.

HRTEM of Pd/ $\text{TiO}_2\text{-C}$ (Fig. 1) details the lattice structure of the material. The lattice parameters, found by indexing the selected area electron diffraction (SAED) pattern (Fig. 1(b)) using a zone axis of [001],

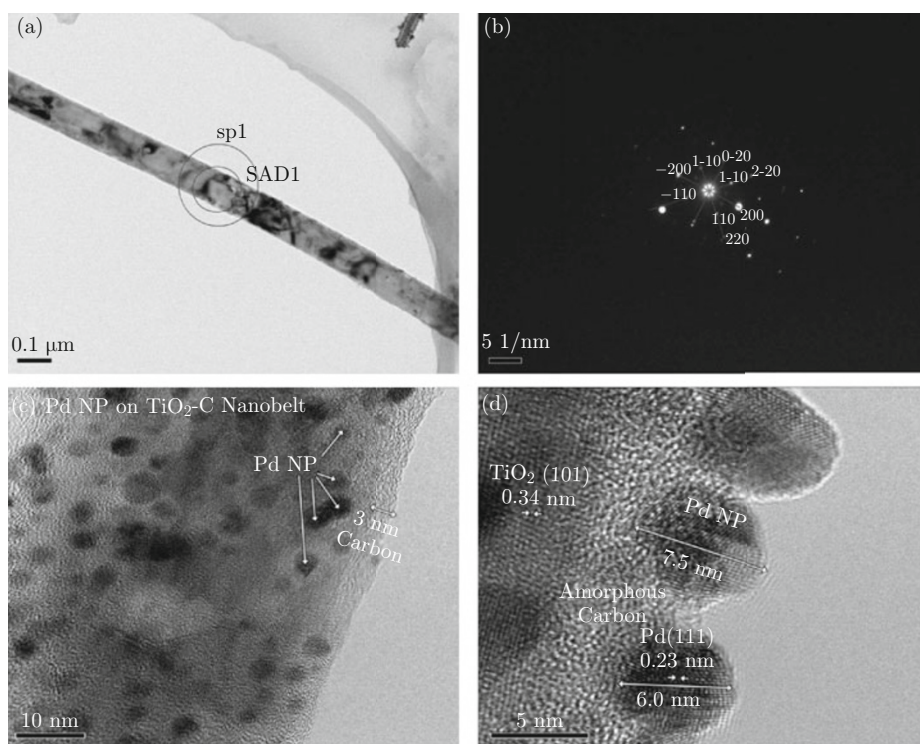


Fig. 1 TEM Images of Pd/ $\text{TiO}_2\text{-C}$ nanobelts: (a) Single Pd/ $\text{TiO}_2\text{-C}$ nanobelts; (b) Indexed SAED patterns with the zone axis of [001]; (c) High resolution image of $\text{TiO}_2\text{-C}$ nanobelt coated with a 3 nm amorphous carbon layer and deposited Pd nanoparticles; and (d) visible 6-8 nm Pd (111) nanoparticles on TiO_2 (101) planes with amorphous carbon phases.

is mostly attributed to the anatase phase (tetragonal structure), in agreement with the XRD results given below. HRTEM observation also reveals the existence of a 3 nm amorphous carbon layer in Fig. 1(c), and spherical Pd nanoparticles (Fig. 1(c) and 1(d)) with a mean diameter less than 10 nm.

FE-SEM images (Fig. 2) indicate that Pd/TiO₂-C nanobelts (Fig. 2(a)) and Pd/TiO₂ nanobelts (Fig. 2(b)) have similar morphology with decorated Pd

nanoparticles; however TiO₂-C has a coated layer of carbon from the carbonization process shown in Fig. 1. The nanobelts have a thickness of around 20-40 nm with a width of 50-200 nm and a length that ranges up to several tens of micrometers. In addition to the two TiO₂ samples, activated carbon decorated with Pd nanoparticles is depicted (Fig. 2(c)), where carbon spheres range from 2-12 μm. The presence of C, Ti, O, and Pd elements was verified through EDX analysis.

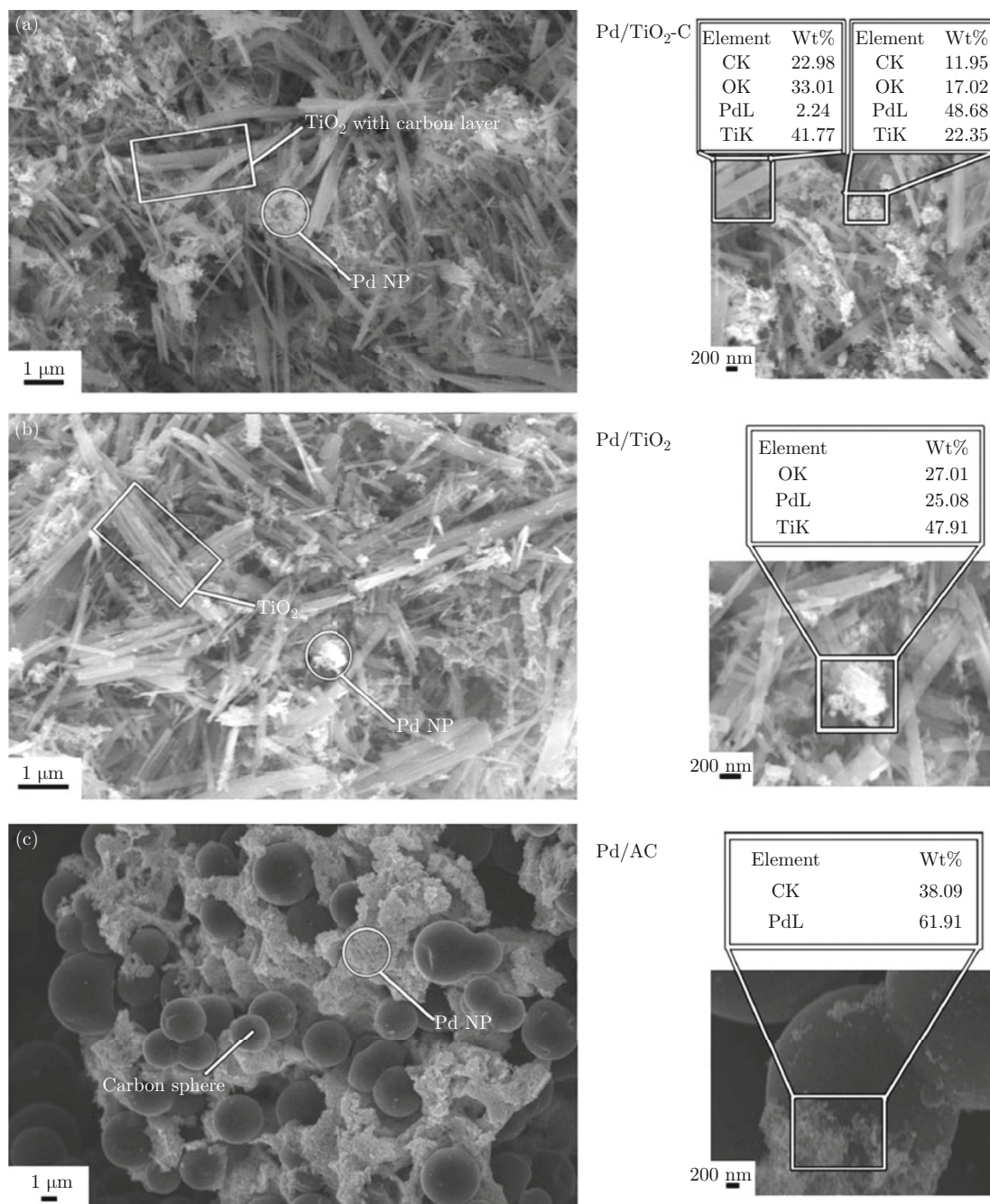


Fig. 2 FE-SEM images with EDX of three samples: (a) Pd/TiO₂-C nanobelts; (b) Pd/TiO₂ nanobelts; (c) Pd/AC. Features in the FE-SEM images are highlighted and EDX elemental composition results and their respective scanned region are given.

XRD patterns of Pd/TiO₂-C, Pd/TiO₂, and Pd/AC samples are shown in Fig. 3. In all of the catalysts, four characteristic diffraction peaks at near 40°(111), 46°(200), 68°(220), and 81°(311) are observed and belong to the face-centered cubic (fcc) phase of Pd. Pd/TiO₂ shows characteristic anatase peaks, whereas, Pd/TiO₂-C shows lower intensity anatase peaks due to surface carbon coating.

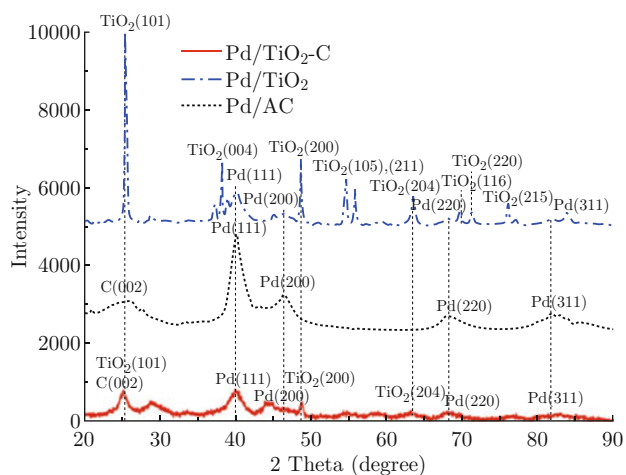


Fig. 3 XRD patterns of three samples: Pd/TiO₂-C, Pd/TiO₂ and Pd/AC.

XPS analysis was performed from 0 to 1200eV for Pd/TiO₂-C and Pd/TiO₂. Ti_{2p}, O_{1s}, C_{1s}, and Pd_{3d} peaks were detected and the peaks were deconvoluted and analyzed for their chemical bonds (Fig. S3) using an online database [37]. From the peaks, all Pd/TiO₂-C spectra are shifted to higher binding energies compared to the Pd/TiO₂ spectra. In the Ti_{2p} spectrum, the separation between the Ti doublets in Pd/TiO₂-C is 5.9 eV (Fig. S3(a)), which is slightly larger than the 5.7 eV separation of Pd/TiO₂ peaks (Fig. S3(b)). The higher binding energies of Ti 2p_{3/2} and Ti 2p_{1/2}, and lower BE splitting for Pd/TiO₂-C may be ascribed to the existence of Ti-O-C [30]. Furthermore, the C_{1s} peak for Pd/TiO₂-C (Fig. S3(e)) has a larger magnitude than the Pd/TiO₂ peak (Fig. S3(f)), indicating a significant amount of carbon on the surface Pd/TiO₂-C sample, after accounting for the use of the C_{1s} peak as a charging reference to correct measure BE in non-conductive samples.

Pd loading was determined using anodic stripping voltammetry with a chitosan modified electrode. Using a calibration curve (Fig. S4(a)), the peak currents (Fig. S4(b)) were used to determine the Pd concentration in each catalyst. As seen in Table 1, the Pd percentage in the catalyst of Pd/TiO₂-C, Pd/TiO₂, and Pd/AC are 12.2±0.4 %, 16.9±0.5 %, and 12.8±0.4 %, respectively.

The conductivity measurements of the catalysts (see Fig. S5) yield values of 3.45 × 10⁻⁵ S/m, 6.20 × 10⁻⁶

S/m, and 21.0 S/m for TiO₂-C, TiO₂, and AC, respectively. Compared to pure TiO₂ nanobelts, there is approximately an order of magnitude improvement in TiO₂-C, which can be attributed to the carbon coating. However, as displayed in TEM images, the coated carbon is mainly amorphous carbon. This results in much weaker conducting performance than AC because of lack of crystallinity. Since an enhanced conductivity can improve the overall energy converting efficiency, a further work is under way to improve the conductivity of the carbon coating layer.

Electrocatalytic performance

Cyclic voltammetry in alkaline solution

Base CV experiments of Pd/TiO₂-C, Pd/TiO₂, and Pd/AC catalysts were conducted in a solution of 1.0 M KOH and purged in nitrogen as seen in Fig. 4, where the inset figure corresponds to the cyclic voltammograms of the supports without Pd, which include TiO₂-C, TiO₂, and AC, and their capacitive contribution. During the oxidation current potential sweep, in the range between -1.0 V and -0.4 V, desorption and oxidation of adsorbed and absorbed hydrogen occurs [38,39]:

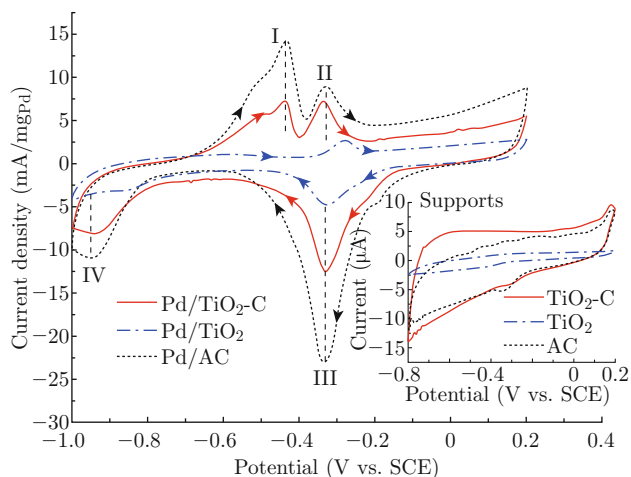
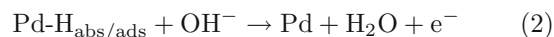
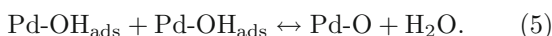
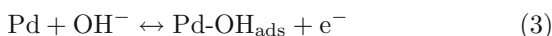


Fig. 4 Cyclic voltammograms of all catalysts (Pd/TiO₂-C, Pd/TiO₂ and Pd/AC) in a solution of 1.0 M KOH at a scan rate of 50 mV/s. The inset figure corresponds to the cyclic voltammograms of the catalyst supports, which include TiO₂-C, TiO₂ and AC.

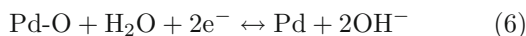
For the Pd/TiO₂-C and Pd/AC samples, peak I corresponds to hydrogen desorption and/or oxidation in this region, but does seem to appear in the Pd/TiO₂ sample because of the inherent low hydrogen adsorption capacity.

From the forward scan, peak II, which emerges at a potential of -0.4 V, correspond to the formation of Pd oxides and partially overlaps the hydrogen desorption

peak. The process of the oxidation process is unclear, but it is accepted that the process initially starts with chemisorbed OH^- ions on Pd that can be transformed into higher valence Pd oxides at higher potentials [38-42]:



Peak III, centered at -0.33 V, can be attributed to the reduction of Pd oxide during the reduction sweep [34,38],



Following the reduction sweep, peak IV (-0.8 V to -1.0 V) corresponds to the adsorption of hydrogen. From the Pd oxide peaks, the EASA values, obtained using Eq. (1), were $99.1 \text{ cm}^2/\text{mg}$, $30.8 \text{ cm}^2/\text{mg}$, and $181.3 \text{ cm}^2/\text{mg}$ for Pd/TiO₂-C, Pd/TiO₂, and Pd/AC, respectively. The Pd/TiO₂-C:Pd/AC EASA ratio is 0.5, whereas the Pd/TiO₂-C:Pd/TiO₂EASA ratio is 3.2. The difference in EASA between the Pd/TiO₂-C and Pd/TiO₂ may be due to the added electrical conductivity of adding carbon to TiO₂-C, which was exhibited in the conductivity tests on powdered samples and is a factor in the contribution of increasing EASA in the Pd/TiO₂-C catalyst.

Cyclic voltammetry in alkaline methanol solution

In Fig. 5, CV curves of Pd/TiO₂-C, Pd/TiO₂, and Pd/AC in a solution of 1 M KOH and 1 M MeOH were obtained to determine electrocatalytic performance. From the CV curves, the Pd/TiO₂-C catalyst exhibits

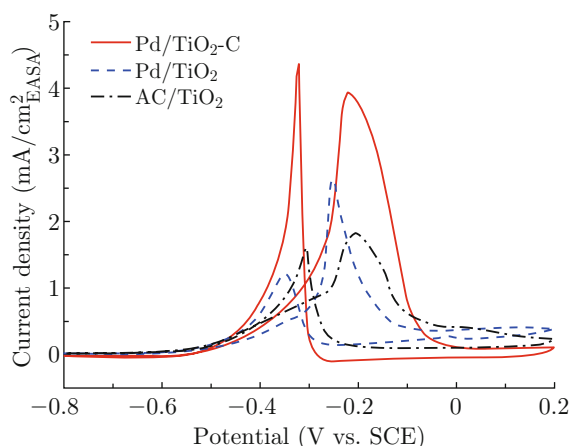


Fig. 5 Cyclic voltammograms (specific activity ($\text{mA}/\text{cm}^2_{\text{EASA}}$) vs. potential (V vs. SCE)) of all catalysts (Pd/TiO₂-C, Pd/TiO₂ and Pd/AC) and supports (TiO₂-C, TiO₂ and AC) in a solution of 1.0 M KOH + 1.0 M MeOH at a scan rate of 50 mV/s.

enhanced catalytic performance compared to Pd/TiO₂ and Pd/AC over the potential range of 0.2 V to -0.8 V with respect to SCE electrode. In the forward scan, the oxidation peak corresponds to the oxidation of chemisorbed species from methanol adsorption. The reverse scan peak is associated with desorption and oxidation of carbonaceous species [43].

The peak current and onset potential on the forward scan indicates the electrocatalytic activity of the catalyst for methanol oxidation. The onset of methanol oxidation occurs at -0.595 V vs. SCE for Pd/TiO₂-C and -0.545 V vs. SCE for Pd/TiO₂, whereas it is -0.600 V vs. SCE for Pd/AC. Pd/TiO₂-C has a similar onset potential to Pd/AC, but a lower onset potential than Pd/TiO₂, suggesting that the electrocatalytic activity towards methanol oxidation occurs more favorably in Pd/TiO₂-C and Pd/AC than in Pd/TiO₂ [44]. When comparing specific activities (Fig. 5), Pd/TiO₂-C has a peak current density ($3.93 \text{ mA}/\text{cm}^2_{\text{EASA}}$) that is 2.2 times that of Pd/AC ($1.80 \text{ mA}/\text{cm}^2$) and 1.5 times that of Pd/TiO₂ ($2.63 \text{ mA}/\text{cm}^2_{\text{EASA}}$). The magnitude of the current density, and thus the magnitude of methanol oxidation, is greater in both Pd/TiO₂-C and Pd/TiO₂ samples than Pd/AC when taking into account the EASA.

Figure 6 shows the peak current densities at various methanol concentrations from 0.1 M to 4 M of catalysts in the forward scan. An inverse exponential decay function is generally observed for all catalyst curves within the methanol concentration range and this function follows the Langmuir adsorption model, where the current density is dictated by the surface coverage of the alcohol and hydroxyl adsorbates [36]. From Fig. 6, at all concentrations, Pd/TiO₂-C was found to have about 2.5 times the specific activity of Pd/AC and 1.5 times the specific activity of Pd/TiO₂.

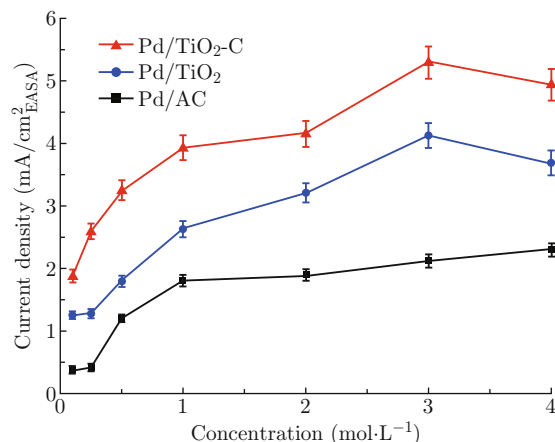


Fig. 6 Peak current density ($\text{mA}/\text{cm}^2_{\text{EASA}}$) in the forward scan for all catalysts (Pd/TiO₂-C, Pd/TiO₂ and Pd/AC) at MeOH concentrations from 0.1 M to 4.0 M.

F. Hu *et al.* conducted a similar study for electrooxidation of alcohols, except using carbonized TiO₂ nanotubes instead of TiO₂ nanobelts [23]. In their study, methanol electrooxidation was conducted in 1.0 M KOH and 1.0 M MeOH. From the cyclic voltammetry results, Pd/TiO₂-C nanotubes had a peak current density of 133 mA/mg_{Pd}, which was 1.75 times greater than the peak density of Pd/C (76 mA/mg_{Pd}) and 4.43 times greater than the peak density of Pd/TiO₂ nanotubes (30 mA/mg_{Pd}). As a comparison, the Pd/TiO₂-C nanobelts in this study demonstrate a higher absolute peak current density than that of F. Hu *et al.*, but a lower peak density ratio when compared to carbon support used. However, this may be attributed to several factors rather than TiO₂ structure alone, such as the Pd synthesis process and the carbonization process. The EASA requires that the Pd catalyst should be present at the surface so it is exposed to the Nafion layer and the methanol-electrolyte solution. Methanol and other reactant species diffuse through the Nafion film and react with specific Pd catalyst planes on the surface [45]. It is also known that structurally defective or rough (stepped) surfaces are better candidates for effective catalysis than perfect (111) facets of fcc cubic structures for Pd and Pt [46]. Therefore, the Pd synthesis process on the catalyst surface is a factor that should be considered to explain the disparity between the current densities. Furthermore, the discrepancy in results may also be attributed to the differences in the carbonization process of the catalysts, since surface conductivity changes with different processing conditions and this may lead to varying catalytic performances.

Electrocatalytic stability-chronoamperometry and long cycle cyclic voltammetry

A catalyst's stability as a function of time is also

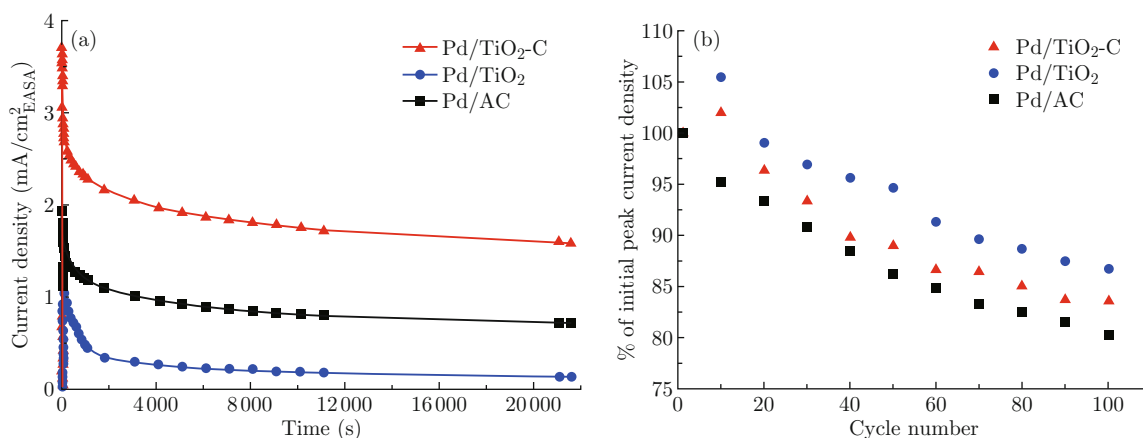


Fig. 7 (a) Chronoamperometry curves (specific Activity (mA/cm²_{EASA}) vs. time (s)) of all catalysts (Pd/TiO₂-C, Pd/TiO₂ and Pd/AC) conducted in a solution of 1 M KOH and 1 M MeOH collected at -0.2 V vs. SCE; (b) Plot of % initial peak current density vs. cycle number using Pd/TiO₂-C, Pd/TiO₂, and Pd/AC catalysts conducted using cyclic voltammetry in a solution of 1 M KOH and 1 M MeOH collected at -0.2 V vs. SCE (scan rate 50 mV/s).

important for their practical application in DMFCs and was investigated using an electrochemical cell with a three-electrode setup. To probe the stability of the catalysts, the current densities were observed at a constant potential of -0.2 V vs. SCE and under cyclic voltammetry for 100 cycles. As observed in Fig. 7(a), the current density of methanol oxidation drops quickly within the first 5-10 min of all samples possibly due to the formation of Pd oxides (PtO_x) as shown in Fig. 4. The initial deactivation of the catalyst is a quasi-reversible process and partial recovery of catalytic activity may be obtained by cycling to a lower potential periodically [47,48]. The long term poisoning rate from these adsorbed species, δ , can be described as the linear decay of the current density obtained from chronoamperometry after 500 s and is given by [49]:

$$\delta = \frac{100}{I_o} \left(\frac{dI}{dt} \right)_{t>500} \quad (7)$$

where $(dI/dt)_{t>500}$ is the slope of the linear portion of the current decay, and I_o is the current at the start of polarization back extrapolated from the linear current decay. The calculated δ values are given in Table 2. Of note, is the one-order magnitude lower poisoning rate of Pd/TiO₂ compared to Pd/TiO₂-C and Pd/AC. Although the poisoning rate of Pd/TiO₂-C is similar to Pd/AC, the initial and final methanol oxidation currents for the Pd/TiO₂-C catalyst are superior to that of Pd/AC. For instance, from a specific activity standpoint, the final methanol oxidation current of Pd/TiO₂-C at 21600 seconds (6 h) is approximately 2.19 times greater than that of Pd/AC and 12.2 times greater than that of Pd/TiO₂, demonstrating the higher methanol oxidation rate of Pd/TiO₂-C.

Table 2 The long-term poisoning rate for Pd/TiO₂-C, Pd/TiO₂, and Pd/AC catalysts.

| Catalyst | Poisoning Rate (δ , % per s) |
|------------------------|---|
| Pd/TiO ₂ -C | 1.76×10^{-2} |
| Pd/TiO ₂ | 4.67×10^{-3} |
| Pd/AC | 2.29×10^{-2} |

When observing the peak current density of the catalysts as a function of the number of cycles (Fig. 7(b)), the peak current density decays over 100 cyclic voltammetry cycles. The peak current density decay after 100 cycles was 17%, 13%, and 20% for Pd/TiO₂-C, Pd/TiO₂, and Pd/AC, respectively. The current density decay is highest for Pd/AC and lowest for Pd/TiO₂, which follows the trend from the poisoning rates obtained from chronoamperometry curves.

Conclusions

We have demonstrated that carbon modified TiO₂ nanobelts were a viable support material for a Pd catalyst undergoing methanol electrooxidation. These nanobelts have advantages over bare TiO₂ nanobelts in that they slightly improve conductivity of the support and electrocatalytic performance from both a mass activity and specific activity standpoint. In addition, during chronoamperometry in alkaline media, Pd/TiO₂-C was similar in stability to activated carbon, but has an overall higher methanol oxidation current density throughout the entire reaction time. The modification of metal oxide nanostructures, particularly TiO₂ with carbon particles is a viable method, with optimization, to create promising electrocatalyst support candidates for fuel cell and battery applications.

Acknowledgements

This work is supported by FedDev Ontario through the Applied Research and Commercialization (ARC) Initiative and the Natural Sciences and Engineering Research Council of Canada (NSERC) program. We would also like thank Microbonds, Inc. for additional financial support. TEM research described in this paper was performed at the Canadian Centre for Electron Microscopy at McMaster University.

References

- [1] M. Zhiani, B. Rezaei and J. Jalili, "Methanol electrooxidation on Pt/C modified by polyaniline nanofibers for DMFC applications", *Int. J. Hydrogen Energy* 35(17), 9298-9305 (2010). <http://dx.doi.org/10.1016/j.ijhydene.2010.03.050>
- [2] W. Wang, Q. Huang, J. Liu, Z. Zou, Z. Li and H. Yang, "One-step synthesis of carbon-supported Pd-Pt alloy electrocatalysts for methanol tolerant oxygen reduction", *Electrochem. Commun.* 10(9), 1396-1399 (2008). <http://dx.doi.org/10.1016/j.elecom.2008.07.018>
- [3] H. B. Zhao, J. Yang, L. Li, H. Li, J. L. Wang and Y. M. Zhang, "Effect of over-oxidation treatment of Pt-Co/polypyrrole-carbon nanotube catalysts on methanol oxidation", *Int. J. Hydrogen Energy* 34(9), 3908-3914 (2009). <http://dx.doi.org/10.1016/j.ijhydene.2009.02.079>
- [4] W. Q. Zhou, C. Y. Zhai, Y. K. Du, J. K. Xu and P. Yang, "Electrochemical fabrication of novel platinum-poly(5-nitroindole) composite catalyst and its application for methanol oxidation in alkaline medium", *Int. J. Hydrogen Energy* 34(23), 9315-9323 (2009). <http://dx.doi.org/10.1016/j.ijhydene.2009.09.059>
- [5] W. Q. Zhou, Y. K. Du, F. F. Ren, C. Y. Wang, J. K. Xu and P. Yang, "High efficient electrocatalytic oxidation of methanol on Pt/polyindoles composite catalysts", *Int. J. Hydrogen Energy* 35(8), 3270-3279 (2010). <http://dx.doi.org/10.1016/j.ijhydene.2010.01.083>
- [6] H. Zhang, W. Zhou, Y. Du, P. Yang, C. Wang and J. Xu, "Enhanced electrocatalytic performance for methanol oxidation on Pt-TiO₂/ITO electrode under UV illumination", *Int. J. Hydrogen Energy* 35(24), 13290-13297 (2010). <http://dx.doi.org/10.1016/j.ijhydene.2010.09.025>
- [7] A. V. Tripkovic, K. Dj. Popovic, J. D. Lovic, V. M. Jovanovic and A. Kowal, "Methanol oxidation at platinum electrodes in alkaline solution: comparison between supported catalysts and model systems", *J. Electro. Chem.* 572(1), 119-128 (2004). <http://dx.doi.org/10.1016/j.jelechem.2004.06.007>
- [8] H. Wang, M. Zhang, F. Cheng and C. Xu, "Pt supported on Ti for methanol electrooxidation by magnetron sputter method", *Int. J. Electrochem. Sci.* 3, 946 (2008). <http://www.electrochemsci.org/papers/vol3/3080946.pdf>
- [9] R. G. Freitas, M. C. Santos, R. T. S. Oliveira, L. O. S. Bulhoes and E. C. Pereira, "Methanol and ethanol electrooxidation using Pt electrodes prepared by the polymeric precursor method", *J. Power Sources* 158(1), 164-168 (2006). <http://dx.doi.org/10.1016/j.jpowsour.2005.10.002>
- [10] B. Liu, J. H. Chen, C. H. Xiao, K. Z. Cui, L. Yang, H. L. Pang and Y. F. Kuang, "Preparation of Pt/MgO/CNT hybrid catalysts and their electrocatalytic properties for ethanol electrooxidation", *Energy & Fuels* 21(3), 1365-1369 (2007). <http://dx.doi.org/10.1021/ef060452i>
- [11] N. Jha, A. L. M. Reddy, M. M. Shaijumon, N. Rajalakshmi and S. Ramaprabhu, "Pt-Ru/multi-walled carbon nanotubes as electrocatalysts for direct methanol fuel cell", *Int. J. Hydrogen Energy* 33(1), 427-433 (2008). <http://dx.doi.org/10.1016/j.ijhydene.2007.07.064>
- [12] E. H. Yu, K. Scott and R. W. Reeve, "A study of the anodic oxidation of methanol on

- Pt in alkaline solutions”, *J. Electroanal. Chem.* 547(1), 17-24 (2003). [http://dx.doi.org/10.1016/S0022-0728\(03\)00172-4](http://dx.doi.org/10.1016/S0022-0728(03)00172-4)
- [13] Q. He, W. Chen, S. Mukerjee, S. Chen and F. Laufek, “Carbon-supported PdM (M = Au and Sn) nanocatalysts for the electrooxidation of ethanol in high pH media”, *J. Power Sources* 187(2), 298-304 (2009). <http://dx.doi.org/10.1016/j.jpowsour.2008.11.065>
- [14] Deffernez, S. Hermans and M. Devillers, “Bimetallic Bi-Pt, Ru-Pt and Ru-Pd and trimetallic catalysts for the selective oxidation of glyoxal into glyoxalic acid in aqueous phase”, *App. Catalysis A: General* 282(1-2), 303-313 (2005). <http://dx.doi.org/10.1016/j.apcata.2004.12.023>
- [15] C. H. Yen, K. Shimizu, Y. Lin, F. Bailey, I. F. Cheng and C. M. Wai, “Chemical fluid deposition of Pt-based bimetallic nanoparticles on multiwalled carbon nanotubes for direct methanol fuel cell application”, *Energy & Fuels* 21(4), 2268-2271 (2007). <http://dx.doi.org/10.1021/ef0606409>
- [16] W. Du, Q. Wang, C. A. LaScala, L. Zhang, D. Su, A. Frenkel, V. K. Mathur and X. Teng, “Ternary PtSnRh-SnO₂ nanoclusters: synthesis and electroactivity for ethanol oxidation fuel cell reaction”, *J. Mater. Chem.* 21, 8887-8892 (2011). <http://dx.doi.org/10.1039/C0JM04358C>
- [17] J. Kim and S. Park, “Electrochemical oxidation of ethanol at thermally prepared RuO₂-Modified electrodes in alkaline media”, *J. Electrochem. Soc.* 146(3), 1075-1080 (1999). <http://dx.doi.org/10.1149/1.1391723>
- [18] Fujishima, T. N. Rao and D. A. Tryk, “Titanium dioxide photocatalysis”, *J. Photochem. Photobiol. C* 1(1), 1-21 (2000). [http://dx.doi.org/10.1016/S1389-5567\(00\)00002-2](http://dx.doi.org/10.1016/S1389-5567(00)00002-2)
- [19] A. R. Gandhe, S. P. Naik and J. B. Fernandes, “Selective synthesis of N-doped mesoporous TiO₂ phases having enhanced photocatalytic activity”, *Microporous Mesoporous Mater.* 87(2), 103-109 (2005). <http://dx.doi.org/10.1016/j.micromeso.2005.07.017>
- [20] Anming Hu, X. Zhang, K. D. Oakes, P. Peng, Y. N. Zhou and M. R. Servos, “Hydrothermal growth of free standing TiO₂ nanowire membranes for photocatalytic degradation of pharmaceuticals”, *J. Hazard. Mater.* 189(1-2), 278-285 (2011). <http://dx.doi.org/10.1016/j.jhazmat.2011.02.033>
- [21] A. Hu, R. Liang, X. Zhang, S. Kurdi, D. Luong, H. Huang, P. Peng, E. Marzbanrad, K. D. Oakes, Y. Zhou and M. R. Servos, “Enhanced photocatalytic degradation of dyes by TiO₂ nanobelts with hierarchical structures”, *J. Photochem. Photobiology A: Chem.* 256, 7-15 (2013). <http://dx.doi.org/10.1016/j.jphotochem.2013.01.015>
- [22] A. Hu, X. Zhang, D. Luong, K. Oakes, M. Servos, R. Liang, S. Kurdi, P. Peng and Y. Zhou, “Adsorption and photocatalytic degradation kinetics of pharmaceuticals by TiO₂ nanowires during water treatment”, *Waste Biomass Valor* 3(4), 443-449 (2012). <http://dx.doi.org/10.1007/s12649-012-9142-6>
- [23] F. Hu, F. Ding, S. Song and P. K. Shen, “Pd electrocatalyst supported on carbonized TiO₂ nanotube for ethanol oxidation”, *J. Power Sources* 163(1), 415-419 (2006). <http://dx.doi.org/10.1016/j.jpowsour.2006.09.039>
- [24] Z. Yang, G. Du, Q. Meng, Z. Guo, X. Yu, Z. Chen, T. Guo and R. Zeng, “Synthesis of uniform TiO₂@carbon composite nanofibers as anode for lithium ion batteries with enhanced electrochemical performance”, *J. Mater. Chem.* 22, 5848-5854 (2012). <http://dx.doi.org/10.1039/C2JM14852H>
- [25] M. A. Abdelkareem, Y. Ito, T. Tsujiguchi and N. Nakagawa, “Carbon-TiO₂ composite nanofibers as a promising support for PtRu anode catalyst of DMFC”, *ECS Trans.* 50(2), 1959-1967 (2013). <http://dx.doi.org/10.1149/05002.1959ecst>
- [26] A. R. Fakhari, B. Rafiee, H. Ahmar and A. Bagheri, “Electrocatalytic determination of oxalic acid by TiO₂ nanoparticles/multiwalled carbon nanotubes modified electrode”, *Anal. Methods* 4, 3314-3319 (2012). <http://dx.doi.org/10.1039/C2AY25077B>
- [27] F. Zhang, F. Xie, H. Xu, J. Liu and W. C. Oh, “Characterization of Pd/TiO₂ embedded in multi-walled carbon nanotube catalyst with a high photocatalytic activity”, *Kinetics and Catalysts* 54(3), 297-306 (2013). <http://dx.doi.org/10.1134/S002315841303018X>
- [28] D. Guo, X. Qiu, L. Chen and W. Zhu, “Multi-walled carbon nanotubes modified by sulfated TiO₂ - A promising support for Pt catalyst in a direct ethanol fuel cell”, *Carbon* 47(7), 1680-1685 (2009). <http://dx.doi.org/10.1016/j.carbon.2009.02.023>
- [29] Alex Bauer, R. Hui, A. Ignaszak, J. Zhang and D. Jones, “Application of a composite structure of carbon nanoparticles and Nb-TiO₂ nanofibers as electrocatalyst support for PEM fuel cells”, *J. Power Sources* 210, 15-20 (2012). <http://dx.doi.org/10.1016/j.jpowsour.2012.02.093>
- [30] Z. Yang, G. Du, Z. Guo, X. Yu, Z. Chen, T. Guo and R. Zeng, “Encapsulation of TiO₂(B) nanowire cores into SnO₂/carbon nanoparticle shells and their high performance in lithium storage”, *Nanoscale* 3, 4440-4447 (2011). <http://dx.doi.org/10.1039/C1NR10837A>
- [31] X. Wang, J. Wang, Q. Zou and Y. Xia, “Pd nanoparticles supported on carbon-modified rutile TiO₂ as a highly efficient catalyst for formic acid electrooxidation”, *Electrochimica Acta* 56, 1646-1651 (2011). <http://dx.doi.org/10.1016/j.electacta.2010.08.003>
- [32] Y. L. Hsin, K. C. Hwang and C. Yeh, “Poly(vinylpyrrolidone)-modified graphite carbon nanofibers as promising supports for PtRu catalysts in direct methanol fuel cells”, *J. Am. Chem. Soc.* 129(32), 9999-10010 (2007). <http://dx.doi.org/10.1021/ja072367a>
- [33] S. S. Mahapatra and J. Datta, “Characterization of Pt-Pd/C electrocatalyst for methanol oxidation in alkaline medium”, *Int. J. Electrochem.* 2011, Article ID: 563495 (2011). <http://dx.doi.org/10.4061/2011/563495>

- [34] R. N. Singh, A. Singh and Anindita, "Electrocatalytic activity of binary and ternary composite films of Pd, MWCNT and Ni, Part II: Methanol electrooxidation in 1 M KOH", *Int. J. Hydrogen Energy* 34(4), 2052-2057 (2009). <http://dx.doi.org/10.1016/j.ijhydene.2008.12.047>
- [35] G. Xue, Y. Gui, T. Yu, J. Guan, X. Yu, J. Zhang, J. Liu and Z. Zou, "Degradation mechanisms investigation for long-term thermal stability of dye-sensitized solar cells", *Int. J. Electrochem. Sci.* 7, 1496-1511 (2012). <http://www.electrochemsci.org/papers/vol7/7021496.pdf>
- [36] Y. Wang, D. C. Alsmeyer and R. L. McCreery, "Raman spectroscopy of carbon materials: structural basis of observed spectra", *Chem. Mater.* 2(5), 557-563 (1990). <http://dx.doi.org/10.1021/cm00011a018>
- [37] XPS database on Web: <http://www.lasurface.com/database/elementxps.php> (Accessed Oct. 2012).
- [38] Z. X. Liang, T. S. Zhao, J. B. Xu and L. D. Zhu, "Mechanism study of the ethanol oxidation reaction on palladium in alkaline media", *Electrochimica Acta* 54, 2203 (2009). <http://dx.doi.org/10.1016/j.electacta.2008.10.034>
- [39] M. Grden and A. Czerwinski, "EQCM studies on Pd-Ni alloy oxidation in basic solution", *J. Solid State Electrochem.* 12(4), 375-385 (2008). <http://dx.doi.org/10.1007/s10008-007-0452-8>
- [40] M. C. Jeong, C. H. Pyun and I. H. Yeo, "Voltammetric studies on the palladium oxides in alkaline media", *J. Electrochem. Soc.* 140(7), 1986-1989 (1993). <http://dx.doi.org/10.1149/1.2220750>
- [41] L. J. Vracar, S. Burojevic and N. Krstajic, "The surface processes at Pd-Ni alloy in acid and alkaline solutions", *Int. J. Hydrogen Energy* 23(12), 1157-1164 (1998). [http://dx.doi.org/10.1016/S0360-3199\(97\)00176-6](http://dx.doi.org/10.1016/S0360-3199(97)00176-6)
- [42] T. Takamura and K. Minamiya, "Anodic oxidation of methanol at palladium electrode in alkaline solution", *J. Electrochem. Soc.* 112(3), 333-335 (1965). <http://dx.doi.org/10.1149/1.2423534>
- [43] C. Xu, Y. Liu and D. Yuan, "Pt and Pd supported on carbon microspheres for alcohol electrooxidation in alkaline media", *Int. J. Electrochem. Sci.* 2, 674-680 (2007). <http://www.electrochemsci.org/papers/vol2/2090674.pdf>
- [44] Z. Shih, C. Wang, G. Xu and H. Chang, "Porous palladium copper nanoparticles for the electrocatalytic oxidation of methanol in direct methanol fuel cells", *J. Mater. Chem. A* 1(15), 4774-4778 (2013). <http://dx.doi.org/10.1039/C3TA01664A>
- [45] Z. Qi, in *PEM Fuel Cell Electrocatalysts and Catalyst Layers*, ed. J. Zhang, Springer-Verlag London Limited, ch.11, 547 (2008).
- [46] G. A. Somorjai, "Modern concepts in surface science and heterogeneous catalysis", *J. Phys. Chem.* 94, 1013-1023 (1990). <http://dx.doi.org/10.1021/j100366a001>
- [47] H. Hoster, T. Iwasita, H. Baumgartner and W. Vielstich, "Current-Time behavior of smooth and porous PtRu surfaces for methanol oxidation", *J. Electrochem. Soc.* 148, A496-A501 (2001). <http://dx.doi.org/10.1149/1.1365142>
- [48] J. W. Guo, T. S. Zhao, J. Prabhuram, R. Chen and W. Wong, "Preparation and characterization of a PtRu/C nanocatalyst for direct methanol fuel cells", *J. Electrochem. Acta* 51(4), 754-763 (2005). <http://dx.doi.org/10.1016/j.electacta.2005.05.056>
- [49] J. Jiang and A. Kucernak, "Electrooxidation of small organic molecules on mesoporous precious metal catalysts: II: CO and methanol on platinum-ruthenium alloy", *J. Electroanal. Chem.* 543(2), 187-199 (2003). [http://dx.doi.org/10.1016/S0022-0728\(03\)00046-9](http://dx.doi.org/10.1016/S0022-0728(03)00046-9)